EPJ manuscript No.
(will be inserted by the editor)

Nature of the Peierls- to Mott-insulator transition in 1D

H. Fehske[1], A. P. Kampf[2], M. Sekania[2], and G. Wellein[3]

[1] Institut für Physik, Ernst-Moritz-Arndt Universität Greifswald, D-17487 Greifswald, Germany
[2] Institut für Physik, Theoretische Physik III, Universität Augsburg, 86135 Augsburg, Germany
[3] RRZE, Universität Erlangen, 91058 Erlangen, Germany

February 1, 2008

Abstract. In order to clarify the physics of the crossover from a Peierls band insulator to a correlated Mott-Hubbard insulator, we analyze ground-state and spectral properties of the one-dimensional half-filled Holstein-Hubbard model using quasi-exact numerical techniques. In the adiabatic limit the transition is connected to the band to Mott insulator transition of the ionic Hubbard model. Depending on the strengths of the electron-phonon coupling and the Hubbard interaction the transition is either first order or evolves continuously across an intermediate phase with finite spin, charge, and optical excitation gaps.

PACS. 71.10.Hf , 71.10.Fd, 71.45.Lr, 71.30.+h

1 Introduction

In quasi-one-dimensional materials like halogen-bridged transition metal chain complexes, conjugated polymers, organic charge transfer salts, or inorganic blue bronzes the itinerancy of the electrons strongly competes with electron-electron and electron-phonon interactions, which tend to localize the charge carriers by establishing commensurate spin- (SDW) or charge-density-wave (CDW) ground states (GSs). At half-filling, Peierls (PI) or Mott (MI) insulating phases are favored over the metallic state. Quantum phase transitions between the insulating phases are possible and the character of the electronic excitation spectra reflects the properties of the different insulating GSs. A controversial issue is the nature of the PI-MI transition and whether or not only one quantum critical point separates the PI and MI phases in purely electronic model Hamiltonians [1,2,3,4,5]. Phonon dynamical effects, which are known to be particularly important in low-dimensional materials [6,7] may further modify the transition.

In this paper we study the PI-MI quantum phase transition in the Holstein-Hubbard model (HHM) at half-filling. Exact numerical methods [8] are used to diagonalize the HHM on finite chains, preserving the full dynamics of the phonons, and the density matrix renormalization group (DMRG) technique [9] is applied to the adiabatic HHM and the ionic Hubbard model. On finite periodic chains we identify one critical PI-MI transition point in the HHM where the site-parity of the GS changes and the excitation gap in the optical conductivity closes. In the adiabatic limit two scenarios emerge with a discontinuous transition at strong coupling and two subsequent continuous transitions in the weak coupling regime with the possibility for an intermediate insulating phase with finite spin, charge, and optical excitation gaps.

2 Theoretical models

The paradigm for correlated electron-phonon systems has usually been the one-dimensional HHM defined by

$$H = H_{t-U} - g\omega_0 \sum_{i,\sigma} (b_i^\dagger + b_i) n_{i\sigma} + \omega_0 \sum_i b_i^\dagger b_i \ , \quad (1)$$

$$H_{t-U} = -t \sum_{i,\sigma} (c_{i\sigma}^\dagger c_{i+1\sigma} + \text{H.c.}) + U \sum_i n_{i\uparrow} n_{i\downarrow} \ . \quad (2)$$

H_{t-U} constitutes the conventional Hubbard Hamiltonian with hopping amplitude t and on-site Coulomb repulsion strength U; $c_{i\sigma}^\dagger$ creates a spin-σ electron at Wannier site i and $n_{i\sigma} = c_{i\sigma}^\dagger c_{i\sigma}$. In (1), the second term couples the electrons locally to a phonon created by $b_i^\dagger$. Here $g = \sqrt{\varepsilon_p/\omega_0}$ is a dimensionless electron-phonon coupling constant, where ε_p and ω_0 denote the polaron binding energy and the frequency of the optical phonon mode, respectively.

The GS of the Holstein model for $U = 0$ is a Peierls distorted state with staggered charge order in the adiabatic limit $\omega_0 \to 0$ for any finite ε_p. As in the Holstein model of spinless fermions [10,11], quantum phonon fluctuations destroy the Peierls state for small electron-phonon interaction strength [6] – an issue which has remained unresolved in early studies of the Holstein model using Monte Carlo techniques [12]. Above a critical threshold $g_c(\omega_0)$, the Holstein model describes a PI with equal spin and

charge excitation gaps – the characteristic feature of a band insulator (BI).

The adiabatic limit of the HHM takes the form

$$H = H_{t-U} - \sum_{i,\sigma} \Delta_i n_{i\sigma} + \frac{K}{2} \sum_i \Delta_i^2 \qquad (3)$$

(termed AHHM); it includes the elastic energy of a harmonic lattice with a "stiffness constant" K. In this frozen phonon approach, $\Delta_i = (-1)^i \Delta$ is a measure of the static, staggered density modulations of the PI phase. Eq. (3) with $K = 0$ and fixed Δ is known as the ionic Hubbard model (IHM) for which an insulator-insulator transition was already established before, although with controversial results regarding the possibility of an additional intervening phase [1,2,3]. Interestingly, the IHM was motivated originally in quite different contexts, i.e. for the description of the neutral to ionic transition in charge transfer salts [13] and ferro-electricity in transition metal oxides [14,15].

3 Numerical results

3.1 Charge- and spin-structure factors

In order to establish the GS properties of the above models and the existence of the PI-MI transition we start with the evaluation of the staggered charge- and spin-structure factors $S_c(\pi)$ and $S_s(\pi)$, respectively,

$$S_c(\pi) = \frac{1}{N} \sum_{j,\sigma\sigma'} (-1)^j \langle (n_{i\sigma} - \frac{1}{2})(n_{i+j,\sigma'} - \frac{1}{2}) \rangle \,,$$

$$S_s(\pi) = \frac{1}{N} \sum_{j} (-1)^j \langle S_i^z S_{i+j}^z \rangle \;,\; S_i^z = \frac{1}{2}(n_{i\uparrow} - n_{i\downarrow}) \,.$$

Results for the U-dependences of $S_c(\pi)$ and $S_s(\pi)$ on an 8-site HHM ring are shown in Fig. 1 for two different phonon frequencies, corresponding to adiabatic and non-adiabatic regimes. The PI regime is characterized by a large (small) charge- (spin-) structure factor. Also shown in Fig. 1 are results for the AHHM [$N = 8$ (Lanczos), $N = 64$ (DMRG)] which will be discussed in Sec. 3.3 Increasing U at fixed ε_p and ω_0, Peierls CDW order is suppressed as becomes manifest from the rapid drop of $S_c(\pi)$ which decreases nearly linearly in the adiabatic regime, but its initial decrease is significantly weaker for higher phonon frequencies. The disappearance of the charge ordering signal is accompanied by a steep rise in $S_s(\pi)$ indicating enhanced antiferromagnetic correlations in the MI phase. The data for $S_c(\pi)$ provide evidence for a critical point U_c at which the CDW order disappears: rather abruptly for adiabatic and smoothly for non-adiabatic phonon frequencies. Above U_c the low-energy physics of the system is qualitatively similar to the pure Hubbard chain; it is governed by gapless spin and massive charge excitations. As compared to the PI phase, the local magnetic moment $L_i(U/t, \varepsilon_p/t, \omega_0/t) \propto \langle (S_i^z)^2 \rangle$ is strongly enhanced (e.g. $L_i(8,2,1)/L_i(0,2,1) \simeq 16.4$).

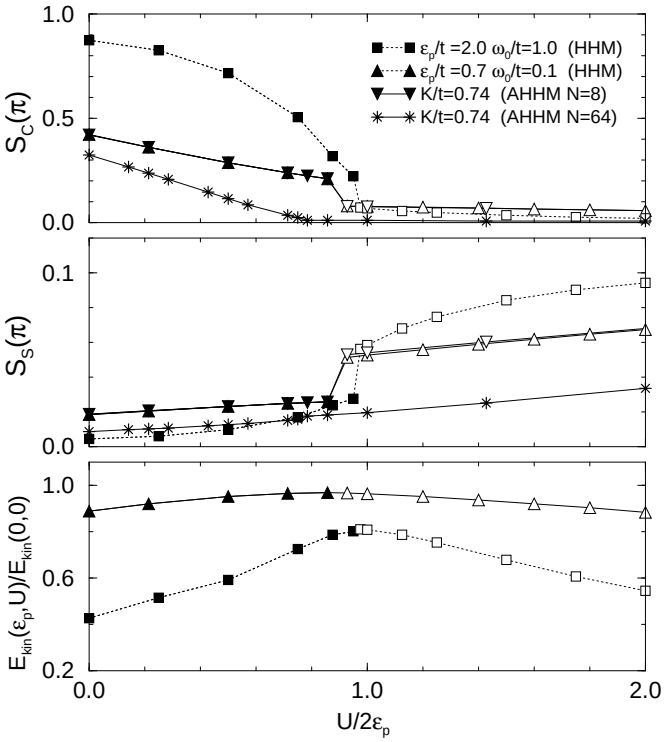

Fig. 1. Staggered charge- (upper) and spin-structure factors (middle panel) vs. the rescaled Hubbard interaction $U/2\varepsilon_p$. The lowest panel displays the U-dependence of the kinetic energy E_{kin}. Lanczos results for the HHM on an 8-site ring are given in the adiabatic (triangles) and non-adiabatic (squares) regimes. Lanczos ($N = 8$ ring, down-triangle) and DMRG (open 64-site chain, stars) results are shown for the AHHM with $K = 0.74$. Open (closed) symbols belong to GSs with site-parity $P = -1$ (+1).

We emphasize the weak finite-size dependence of the exact diagonalization data for $S_c(\pi)$ in both the strong-CDW Peierls and MI phases (see the upper panel of Fig. 2). The variation of $S_s(\pi)$ with the system size N points to a vanishing spin-structure factor in the CDW state, i.e. for $U < U_c$ but, of course, it is beyond our current numerical capabilities to perform a real finite-size analysis for the HHM with dynamical phonons. In the adiabatic limit, we expect a finite $S_s(\pi)$ in the MI phase as for the corresponding SDW state of the so-called extended Hubbard model with $U > 2V$ [16,17].

To discuss the lattice dynamical effects in some more detail we show in Fig. 3 the weights of m-phonon states in the GS of the HHM at different interaction strengths. First of all Fig. 3 demonstrates that our phonon Hilbert space truncation procedure is well-controlled in the sense that states with larger numbers of phonons, as accounted for in the calculations, have negligible spectral weight. Of course, the number of phonons which have to be taken into account strongly depends on the physical situation. Whereas the GS of the MI is almost a zero-phonon state,

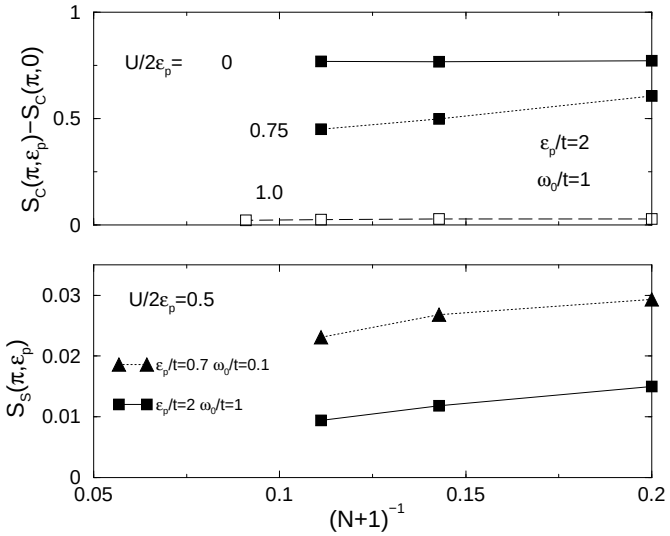

Fig. 2. Finite-size scaling of charge- (upper panel) and spin- (lower panel) structure factors in the HHM.

multi-phonon states become increasingly important if U is reduced (ε_p is enhanced) in the PI regime.

For small U and low phonon frequencies the PI phase appears for $g > g_c(\omega_0)$, even if the ratio $\lambda = \varepsilon_p/2t$ is small. In the GS of such a conventional BI phonons populate predominantly the $q = 0$ and π modes, but the total number of phonons involved in the creation of the Peierls-distorted CDW is rather small. On the contrary, for large phonon frequencies, $g > g_c(\omega_0)$ implies $\lambda \gg 1$ and we observe a multi-phonon GS (cf. Fig. 3). As a consequence the electrons are heavily dressed by phonons, forming bipolarons in real space, which lower their energy by ordering in a staggered CDW. Therefore, in the non-adiabatic strong electron-phonon coupling regime, the system is classified rather as a charge-ordered bipolaronic insulator than as a BI. The kinetic energy is much more suppressed for the bipolaronic than for the band PI (cf. lower panel of Fig. 1). Since SDW correlations reduce E_{kin} as well, the kinetic energy reaches a maximum when the system crosses from the PI to the MI regime.

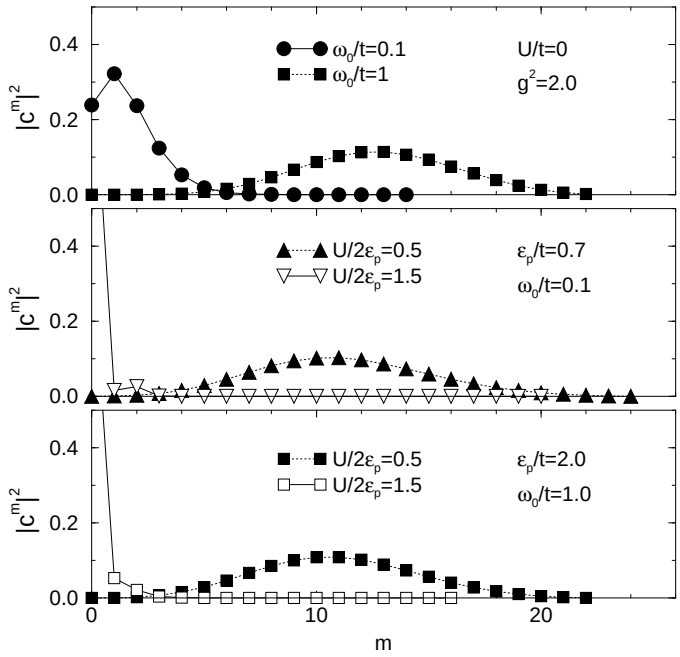

Fig. 3. Phonon distribution in the GS of the HHM for various model parameters. In the MI state (open symbols) the weight of the zero-phonon state is almost one, $|c^m|^2 \simeq 1$.

3.2 Optical response

Valuable insight into the nature of the PI-MI transition is obtained from symmetry considerations [2,5]. The BI-MI transition of the IHM on finite lattices was shown to be connected to a GS level crossing with a site-parity change, where the site inversion symmetry operator P is defined by $Pc^\dagger_{i\sigma}P^\dagger = c^\dagger_{N-i\sigma}$ with $N = 4n$ for $i = 0, ..., N-1$. This feature will become evident in the regular part of the optical conductivity at $T = 0$,

$$\sigma^{reg}(\omega) = \frac{\pi}{N} \sum_{m\neq 0} \frac{|\langle\psi_0|\hat{j}|\psi_m\rangle|^2}{E_m - E_0}\, \delta(\omega - E_m + E_0). \qquad (4)$$

Here, $|\psi_0\rangle$ and $|\psi_m\rangle$ denote the GS and excited states, respectively, and E_m the corresponding eigenenergies. Im-

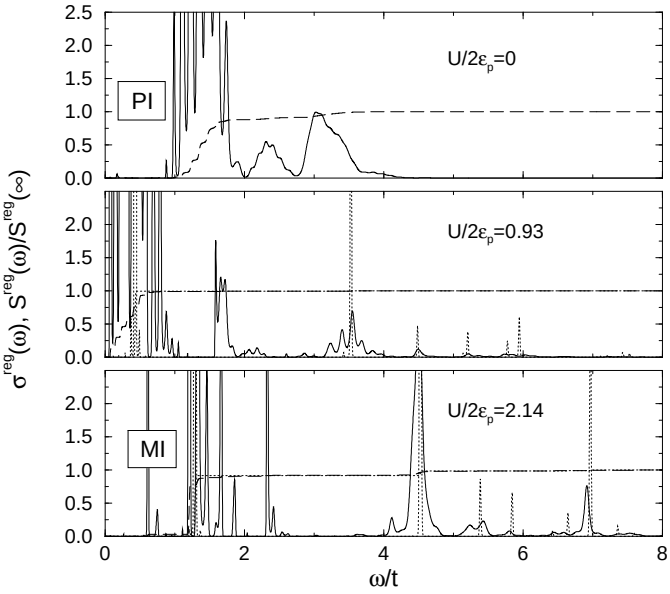

Fig. 4. Optical conductivity in the 8-site HHM for $\omega_0 = 0.1t$ and $g^2 = 7$. Top panel: PI phase for $U = 0$; middle panel: near criticality $U \sim U_{opt}$; lower panel: MI phase for $U = 3t$. Dashed lines give the normalized integrated spectral weights $S^{reg}(\omega)$. The lower two panels include σ^{reg} for $g = 0$ (dotted lines), i.e. for the pure Hubbard chain.

portantly, the current operator $\hat{j} = -\mathrm{i}et\sum_{i\sigma}(c^{\dagger}_{i\sigma}c_{i+1\,\sigma} - c^{\dagger}_{i+1\,\sigma}c_{i\sigma})$ has finite matrix elements between states of different site-parity only.

The evolution of the frequency dependence of $\sigma^{reg}(\omega)$ from the PI to the MI phase with increasing U is illustrated in Fig. 4. In the PI regime the electronic excitations are gapped due to the pronounced CDW correlations. The broad optical absorption band for $U = 0$ results from particle-hole excitations across the BI gap which are accompanied by multi-phonon absorption and emission processes. The shape of the absorption band reflects the phonon distribution function in the GS. Excitonic gap states may occur in the process of structural relaxation. At U_{opt} the optical gap Δ_{opt} closes, and due to the selection rules for optical transitions this necessarily implies a GS level crossing with a site-parity change. We have explicitly verified that the GS site parity in the PI phase is $P = +1$ and $P = -1$ in the MI phase (see also Fig. 1). For the HHM on finite rings U_{opt} is identical to the critical point where $S_c(\pi)$ sharply drops.

For the adiabatic phonon frequency used in Fig. 4 the phonon absorption threshold is small and, because the GS is a multi-phonon state, we find a gradual linear rise of the integrated spectral weight $S^{reg}(\omega) = \int_0^{\omega}\sigma^{reg}(\omega')\,\mathrm{d}\omega'$. $S^{reg}(\omega)/S^{reg}(\infty)$ is a natural measure for the relative weight of the different optical absorption processes. In contrast, in the non-adiabatic regime ($\omega_0 \geq t$), the lowest optical excitations have mainly pure electronic character in the vicinity of U_{opt}. As a result the gap is closed by a state having large electronic spectral weight.

In the MI phase the optical gap is by its nature a correlation gap. The lower panel in Fig. 4 shows clearly that $\sigma(\omega)$ of the HHM in the MI phase is dominated by excitations which can be related to those of the pure Hubbard model. In addition, phononic sidebands with low spectral weight and phonon-induced gap states appear.

3.3 Phase diagram in the adiabatic limit

The above results for the HHM establish the PI-MI phase transition scenario on small rings and trace it to the level crossing of the two site-parity sectors. In order to draw conclusions about the phase diagram in the adiabatic regime we exploit the connection to the AHHM.

The magnitude of $S_c(\pi)$ in the HHM for $U = 0$ and $\omega_0 = 0.1t$ allows a straightforward way to fix the stiffness constant K in Eq. (3). Using the result of the AHHM for $S_c(\pi)$ at $U = K = 0$ we determine first the ionic potential strength Δ_0 by the requirement that $S_c^{IHM}(\pi,\Delta_0) = S_c^{HHM}(\pi)$ for the same chain length and periodic boundary conditions. In a second step, the GS energy of the AHHM, $E_0(K,\Delta,U=0)$, determines K by the criterion that E_0 is minimized for $\Delta = \Delta_0$. We thereby obtain $K = 0.74$, which is henceforth kept fixed when the interaction U is turned on. For each value of U, the ionic potential strength of the AHHM is then obtained by minimizing $E_0(K,\Delta,U)$ with respect to Δ, yielding $\Delta = \Delta(U,K)$ as shown in Fig. 5 (triangles). The resulting structure factors for the AHHM are plotted in Fig. 1, too,

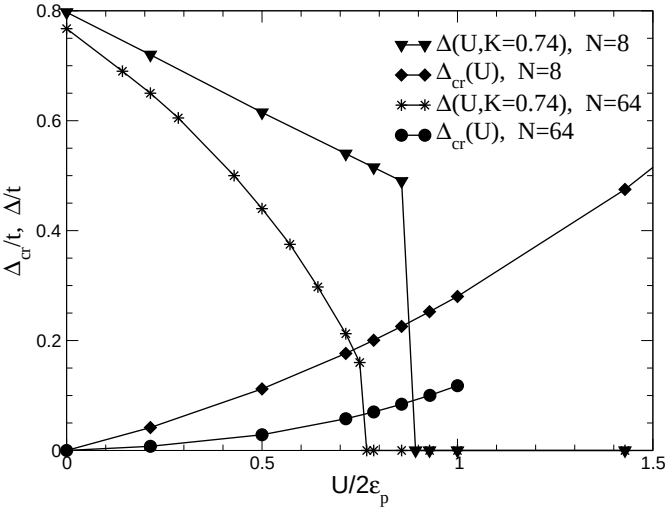

Fig. 5. Level crossing line $\Delta_{cr}(U)$ of the IHM for an 8-site ring (diamonds) and from extrapolating Lanczos data for $N \leq 14$ to a 64-site chain (circles). In addition: ionic potential strength $\Delta(U,K)$ of the AHHM for an 8-site ring (triangles) and on an open 64-site chain (stars, DMRG results) for $K = 0.74$.

and agree very accurately with the 8-site HHM ring data for $\omega_0/t = 0.1$. This agreement reconfirms numerically that the AHHM is indeed the appropriate effective model to describe the CDW phase of the HHM in the adiabatic limit. The drop in $S_c(\pi)$ at the transition point results from a discontinuous vanishing of $\Delta(U,K)$ (see Fig. 5). The large charge structure factor $S_c(\pi)$ below U_c and the enhancement of the spin structure factor $S_s(\pi)$ above U_c as well as the sharp changes at the transition point find a natural explanation with the results for $\Delta(U,K)$ in Fig. 5. Below the transition Δ is finite implying long range CDW order in the GS. At the transition point Δ vanishes discontinuously and thereby the AHHM reduces to the pure Hubbard model ($\Delta = 0$).

Given the value for the stiffness constant K we also plot in Fig. 5 $\Delta(U,K)$ obtained from DMRG on an open chain of length $N = 64$. For comparison, the corresponding results for $S_c(\pi)$ and $S_s(\pi)$ in the AHHM are shown in Fig. 1, too (stars). $S_c(\pi)$ decreases smoothly and almost linearly; although unresolved on the vertical scale in Fig. 1 the transition remains discontinuous as a consequence of the results for $\Delta(U,K)$ in Fig. 5. In contrast to the behavior of the 8-site chain, $\Delta(U,K)$ here decreases more smoothly with increasing U and vanishes discontinuously near $U/2\varepsilon_p \approx 0.75$. The small discontinuous increase in $S_s(\pi)$ at the transition is also hardly resolved for the 64-site chain in contrast to the 8-site chain data. The discontinuous nature of the PI-MI transition in the AHHM for $\Delta_i = (-1)^i\Delta$ is obvious in the atomic limit $t = 0$ where $\Delta = 1/K$ for $U < U_c = 1/K$ and $\Delta = 0$ for $U > U_c$. As verified above, the first order nature persists for finite small t, i.e. in the strong coupling regime $U,\ K^{-1} \gg t$.

Also shown in Fig. 5 is the level crossing line $\Delta_{cr}(U)$ of the IHM for $N = 8$ (diamonds) and $N = 64$ (circles) chain. $\Delta_{cr}(U)$ for $N = 64$ was obtained from extrapolat-

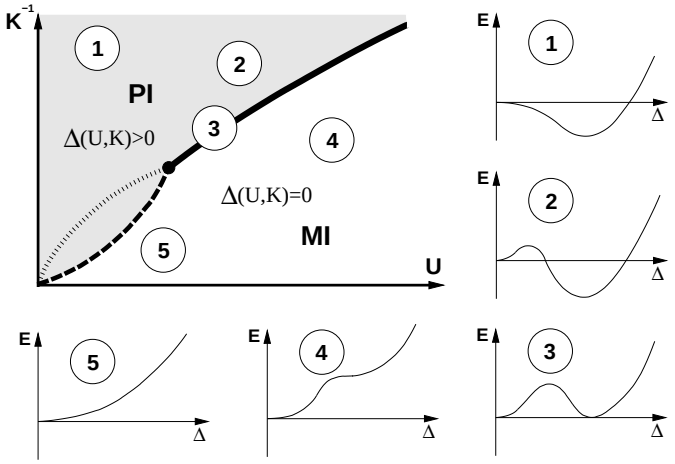

Fig. 6. Insets (1) - (5): Evolution of the ground-state energy vs. Δ in the AHHM in different regions of the (K^{-1}, U) parameter plane. From the variations in $E(\Delta)$ a crossover from a discontinuous PI (with $\Delta > 0$) to MI ($\Delta = 0$) transition to a second order transition is deduced. Main figure: Phase diagram of the AHHM; the solid line represents a discontinuous, first order and the dashed line a continuous second order transition. These results summarize Lanczos data for a 14-site AHHM chain with periodic or open boundary conditions. Detailed runs where performed for $U = 0.3t$ and $U = 5t$. A possible additional continuous transition (dotted line) between two insulating phases with finite Δ is indicated as well.

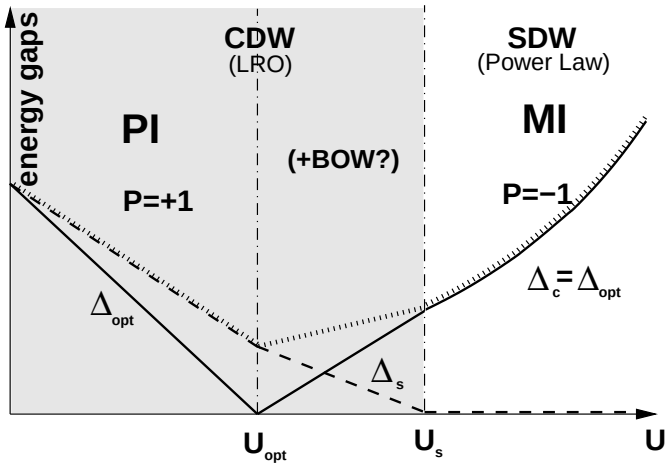

Fig. 7. Qualitative behavior of the excitation gaps versus U in the weak coupling regime of the AHHM $U, K^{-1} \ll t$. Solid line: optical excitation gap Δ_{opt}, dotted line: charge gap Δ_c, dashed line: spin gap Δ_s. PI phase: $\Delta_c = \Delta_s$ and site parity $P = +1$; MI phase: $\Delta_{opt} = \Delta_c$ and $P = -1$.

ing Lanczos results for rings of up to 14 sites to a 64-site chain [18]. Importantly, $\Delta(U, K)$ and $\Delta_{cr}(U)$ do not intercept because $\Delta(U, K)$ jumps to zero before reaching the level crossing point of the IHM.

The DMRG results presented in Fig. 5 for $N = 64$ raise the question whether the discontinuous transition in the AHHM can turn into a continuous transition on approaching the weak coupling regime by increasing the stiffness constant K. Indeed, as we have explicitely verified by exact diagonalization of a periodic (and open too) AHHM ring of length $N = 14$, the transition is second order in the regime $U,\ K^{-1} \ll t$. The corresponding Lanczos results for the variation of the GS energy vs. Δ in the (K, U)-parameter plane are summarized in Fig. 6. Detailed K-scans were performed for weak ($U = 0.3t$) and strong ($U = 5t$) Hubbard interaction. The evolution of $E(\Delta)$ in the AHHM in fact reveals that the transition from the PI to the MI phase (sequence $(2) - (3) - (4)$) occurs discontinuously at strong coupling $K^{-1}, U \gg t$, while the transition follows a Ginzburg-Landau-type behavior for a second order phase transition at weak coupling (sequence $(1) - (5)$ in Fig. 6).

Due to the continuous decrease of $\Delta(U, K)$ at weak coupling $\Delta(U, K)$ necessarily intercepts the $\Delta_{cr}(U)$ line of the IHM [18]. This intercept marks the point U_{opt} when the site-parity sectors become degenerate and the optical absorption gap Δ_{opt} disappears. This situation therefore implies the existence of an intermediate region $U_{opt} < U < U_s$ with finite Δ, where U_s marks the point where Δ continuously vanishes. Since $\Delta = 0$ for $U > U_S$, i.e. when the AHHM reduces to the Hubbard model, the spin gap vanishes at U_s. The intermediate insulating phase thus has finite spin, charge, and optical excitation gaps. For weak coupling the PI-MI transition therefore evolves across two critical points U_{opt} and U_s. The U vs. K^{-1} phase diagram contains a multicritical point at which a first order line splits into two continuous transition lines. The additional transition line is also indicated in Fig. 6 (dotted line). For weak U at fixed K the transition at U_{opt} is expected to be of Kosterlitz-Thouless type since it corresponds to the merging of the energies of the two site-parity sectors; the CDW vanishes in a second order type transition at $U = U_s$. The $E(\Delta)$ behavior, however, can only detect the boundary to the MI phase of the AHHM where the GS energy is minimized for vanishing Δ.

We summarize these findings in the diagram for the excitation gaps shown in Fig. 7,

$$\Delta_c = E_0(N/2+1, N/2) + E_0(N/2-1, N/2) - 2E_0(N/2, N/2)\,, \quad (5)$$

$$\Delta_s = E_0(N/2+1, N/2-1) - E_0(N/2, N/2)\,, \quad (6)$$

where $E_0(N_\uparrow, N_\downarrow)$ is the GS energy of the system with $N_\uparrow$ spin-up and $N_\downarrow$ spin-down electrons. In the Peierls BI phase for $U < U_{opt}$ the spin and charge gaps, are equal and finite and remarkably $\Delta_{opt} \neq \Delta_c$ (for a similar conclusion in the IHM see [20]). At $U = U_{opt}$ the site-parity sectors become degenerate, $\Delta_{opt} = 0$ but remarkably $\Delta_c = \Delta_s > 0$. For $U \geq U_s$ the usual MI phase of the half-filled Hubbard chain with $\Delta_{opt} = \Delta_c > \Delta_s = 0$ is realized. For strong coupling, when the PI to MI transition is first order, $U_{opt} = U_s$, the spin gap discontinuously disappears at the transition and the optical gap jumps from zero to the finite charge gap value of the Hubbard chain. In weak coupling there exists an intermediate region $U_{opt} < U < U_s$ in which all excitation gaps are finite. The CDW persists for all $U < U_s$. The site-parity eigenvalue is $P = +1$ in the PI and $P = -1$ in the MI phase.

The insulating, intermediate phase at weak coupling as identified above remains yet to be characterized. For the insulator-insulator phase transition(s) in the IHM Fabrizio et al. proposed the existence of an intermediate phase with a long range bond order wave (BOW) based on a bosonization analysis [1]. BOW order is characterized by a finite expectation value of the staggered bond charge $B = \frac{1}{N}\sum_{i\sigma}(-1)^i\langle c^\dagger_{i\sigma}c_{i+1\,\sigma} + H.c.\rangle$. Some positive numerical evidence has indeed been reported for enhanced BOW correlations above the level crossing transition in the IHM [3,4,5,21]. Yet, these results have remained ambiguous so far and no consensus has been reached about the existence of long range BOW order in the IHM. In the attempt to search for BOW order the DMRG calculations, which for numerical accuracy reasons are predominantly performed on open chains, suffer from the fact that Friedel-like bond charge density oscillations are induced by the chain ends already for the pure Hubbard chain [5]. The identification of BOW order in the IHM or AHHM by DMRG on open chains therefore requires a delicate subtraction procedure to discriminate a BOW signal from the edge induced bond charge oscillations of the Hubbard chain. We have nevertheless attempted to search for BOW correlations in the weak coupling regime of the AHHM, where the continuous nature of the transition into the MI phase was established by the Lanczos results on the periodic or open 14-sites chain, i.e. these calculations naturally focused on the weak-U regime ($U < t$). This weak coupling regime is notoriously hard for numerical evaluations; unfortunately the numerical accuracy needed to allow a firm conclusion about the presence or absence of a BOW signal could not be achieved within our DMRG runs.

While a confirmation is thus still lacking BOW order remains a vivid candidate order in coexistence with a CDW to characterize the intermediate phase in the AHHM at weak coupling. We furthermore note that if the existence of a BOW is verified in the AHHM, its phase diagram would be remarkably similar to the extended Hubbard model with nearest neighbor Coulomb repulsion with an intervening BOW phase in the crossover between the CDW and MI phases at weak coupling [22,23].

4 Conclusions

In summary, we have found a PI-MI transition in the HHM above a threshold electron-phonon coupling. The transition results from a GS level crossing with a change in the GS site-parity eigenvalue. In the adiabatic limit two scenarios emerge with a discontinuous PI-MI transition for $U, K^{-1} \gg t$, and two continuous transitions for weak coupling $U, K^{-1} \ll t$ with an intermediate phase where CDW order persists. In the non-adiabatic regime our structure factor data indicate that the PI-MI transition proceeds continuously.

Acknowledgments

We appreciate discussions with A.R. Bishop, F. Göhmann, G.I. Japaridze, and A. Weiße. Calculations were performed at the NIC Jülich and the LRZ München, supported by the Bavarian Network for High-Performance Computing (KONWIHR). H.F. and A.P.K. acknowledge support through SPP 1073 and SFB 484 of the Deutsche Forschungsgemeinschaft, respectively.

References

1. M. Fabrizio, A. O. Gogolin, and A. A. Nersesyan, Phys. Rev. Lett. **83**, 2014 (1999); Nucl. Phys. B **580**, 647 (2000).
2. N. Gidopoulos, S. Sorella, and E. Tosatti, Eur. Phys. J. B **14**, 217 (2000).
3. Y. Anusooya-Pati, Z.G. Soos, and A. Painelli, Phys. Rev. B **63**, 205118 (2001).
4. T. Wilkens and R.M. Martin, Phys. Rev. B **63**, 235108 (2001).
5. P. Brune, G.I. Japaridze, A.P. Kampf, and M. Sekania, cond-mat/0106007 v2.
6. E. Jeckelmann, C. Zhang, and S. R. White, Phys. Rev. B **60**, 7950 (1999).
7. H. Fehske, M. Holicki, and A. Weiße, Adv. Sol. State Phys. **40**, 235 (2000).
8. B. Bäuml, G. Wellein, and H. Fehske, Phys. Rev. B **58**, 3663 (1998); A. Weiße, H. Fehske, G. Wellein, and A. R. Bishop, Phys. Rev. B **62**, R747 (2000).
9. S. R. White, Phys. Rev. Lett. **69**, 2863 (1992); Phys. Rev. B **48**, 10345 (1993).
10. R. J. Bursill, R. H. McKenzie, and C. J. Hamer, Phys. Rev. Lett. **80**, 5607 (1998).
11. A. Weiße and H. Fehske, Phys. Rev. B **58**, 13526 (1998).
12. J.E. Hirsch and E. Fradkin, Phys. Rev. B **27**, 4302 (1983).
13. N. Nagaosa and J. Takimoto, J. Phys. Soc. Jpn. **55**, 2735 (1986); N. Nagaosa, ibid. **55**, 2754 (1986).
14. T. Egami, S. Ishihara, and M. Tachiki, Science **261**, 1307 (1993).
15. R. Resta and S. Sorella, Phys. Rev. Lett. **74**, 4738 (1995).
16. B. Fourcade and G. Spronken, Phys. Rev. B **29**, 5089 (1984); Phys. Rev. B **29**.
17. J. E. Hirsch, Phys. Rev. Lett **53**, 2327 (1984).
18. To obtain $\Delta_{cr}(U)$ for rings with $N = 4m+2$ and $N = 4m$ sites we used antiperiodic and periodic boundary conditions, respectively.
19. *Principles of Condensed Matter Physics*, P. M. Chaikin and T. C. Lubensky, Cambridge University Press, 1995, Chapter 4.6.
20. S. Qin, J. Lou, T. Xiang, G. Tian, and Z. Su, preprint cond-mat/0004162 v2.
21. M. E. Torio, A. A. Aligia, and H. A. Ceccatto, Phys. Rev. B **64**,121105 (2001).
22. M. Nakamura, J. Phys. Soc. Jpn. **68**, 3123 (1999); Phys. Rev. B **61**, 16377 (2000).
23. P. Sengupta, A.W. Sandvik, and D.K. Campbell, Phys. Rev. B **65**, 155113 (2002).